Environmental Earth Sciences (2021) 80:649
https://doi.org/10.1007/s12665-021-09939-2

ORIGINAL ARTICLE

Stability analysis of soil-rock slope (SRS) with an improved stochastic method and physical models

Xian-wen Huang[1,2] · Zhi-shu Yao[1] · Wei Wang[3] · Ai-zhao Zhou[2] · Pengming Jiang[2]

Received: 30 July 2020 / Accepted: 1 September 2021 / Published online: 17 September 2021

Abstract

With the development of traffic, many highways were built on the top of soil–rock slope (SRS). However, the effect of highway load on the SRS stability has never been studied comprehensively. Therefore, based on the statistical analysis, the stability of SRS considering additional loads of highway was studied. For generating a more realistic slope model, the identification algorithm of rock characteristic parameters was described considering rock ellipticity and long axis inclination angle; the corresponding rock contour establishing method and SRS establishing process were detailed, which could well consider rock content, ellipticity and long axis inclination angle. Applying the stochastic program, 522 stochastic numerical models and corresponding 12 physical models were created to study the influence of rock contents and long axis inclination angles on the SRS stability. The obtained results showed that the additional loads and dispersion degrees of stochastic analyzing results increased with the increase of rock contents, which were related to plastic developing modes (detour, through, scatter and contain modes) of SRS. By adjusting long axis inclination angles of rocks, it was observed that the minimum or maximum additional load was, respectively, obtained when this angle was parallel with or vertical to plastic belt. The effect of long axis inclination angles to the additional load (30.5%, 38.3% and 60.8% for 20%, 40% and 60% rock content) were concluded, which proved the necessity to consider long axis inclination angles of rocks in estimating SRS stability, especially in high rock content. According to numerical analysis results and the failure characteristic of physical models, three typical development modes of plastic belt of SRS were concluded when the load was on the top of slope, including deep, shallow and partial failure of SRS. In addition, it can also be found that the sliding body shows collapse (whole) modes when long axis inclination angles for rocks are vertical (parallel) to the plastic belt.

Keywords Soil–rock slope · Stochastic method · Additional load · Rock content · Long axis inclination angles of rocks

✉ Zhi-shu Yao
zsyao@aust.edu.cn

Xian-wen Huang
huangxianwen194@163.com

Wei Wang
wellswang@usx.edu.cn

Ai-zhao Zhou
zhouaizhao@126.com

Pengming Jiang
jkdkjcjpm@163.com

[1] School of Architecture and Civil Engineering, Anhui University of Science and Technology, Huainan, Anhui, China

[2] School of Architecture and Civil Engineering, Jiangsu University of Science and Technology, Mengxi Road, Zhenjiang, Jiangsu, China

[3] School of Architecture and Civil Engineering, Shaoxing University, Shaoxing 312000, Zhejiang, China

Introduction

Soil-Rock Slope (SRS) is a heterogeneous slope composed of large and high strength rocks and low strength soil (Kalender et al. 2014; Napoli et al. 2018). Due to the material non-uniformity of rock and soil, the stability and failure modes of SRS are different from the traditional uniform slope (Zhou et al. 2020). It is a geological structure common in Quaternary loose accumulation layers, mainly formed by weathering and residual, landslide collapse and flooding accumulation (Vessia et al. 2017; Zhou et al. 2020). In China, SRS has wide distributions in the Three Gorges area of Yangtze River, Qinghai-Tibet Plateau and southeastern coastal areas (Bao et al. 2015; Huang and Gu 2017). In recent years, with the continuous development of urban and traffic constructions, various highway subways were built on the top of SRS (about 25% of roads were built on SRS).

However, the effect of highway load on the SRS stability had never been studied comprehensively. Therefore, it is necessary to study the SRS stability with additional load for better supporting the engineering construction.

In the past decades, for estimating the SRS stability, three typical methods were concluded, including in-situ test (Coli et al. 2011; Jiang et al. 2018), scale model test (Khorasani et al. 2019), and numerical analysis (Liu et al. 2018a,b). There is no doubt that in-situ test is the best method to analyze SRS stability (Gao et al. 2018; He et al. 2012; Jiang et al. 2018). However, due to the limit of in-situ conditions and investments, in-situ SRS test has been less reported so far. Compared to the in-situ test, scale model test is also a good way to analyze the SRS stability, which has more precise control of research variables and can well predict the stability of the slope (Khorasani et al. 2019; Wu et al. 2015). In scale model tests, two affecting factors should be observed, including (1) the control of model scale (model size, material strength and so on) that the scale model of SRS should be related to the original slope and (2) the quality control of sample preparing (material uniformity, density and so on) which has an important impact on the calculation results. Due to the influence of scale effect and sample preparing non-uniformity, when studying the SRS stability through scale model test, scholars tended to analyze the SRS stability in terms of failure modes (Khorasani et al. 2019; Wang and Zhang 2019). Hence, the scale model test is recognized as a great method to study the failure modes of SRS, which can indirectly support SRS numerical analysis.

Owing to the development of computer technology and analytical theory, great progress has been made in numerical analysis for SRS. Scholars have conducted lots of studies on the SRS stability by numerical analysis and put forward many different numerical models (He et al. 2012; Manouchehrian et al. 2013). In numerical analysis, establishing suitable analytical models for SRS is of great importance and has great influence on the evaluation of slope stability. Liu et al. (2018a,b) meshed slope models and then transformed part soil elements into rock elements (through material properties adjustments) to generate corresponding SRS. Through this method, they could better consider rock content characteristics, but neglected the effect of rock distribution on SRS stability. For solving this, Yang et al. (Meng et al. 2019; Yang et al. 2019a,b) developed a SRS contour algorithm capable of considering large rocks, but rocks were considered as rectangles or circles ignoring the effect of rock shape on SRS stability. Then, Liu et al. (2018a,b) adopted MATLAB software to create a SRS contour algorithm, which could consider the effects of the content, size, shape and location of rocks, but could not establish rock distribution models considering interlock effect between large scale rocks (Meng et al. 2018; Zhang 2017). Liu's model is different from real distribution characteristics of rocks in slopes and will lead to the error of slope stability evaluation results. Therefore, on the basis of numerical analysis, it is necessary to propose a stochastic method which can not only take into account the effects of different shapes and distribution characteristic of rocks, but also consider interlock effect between large scale rocks to study the SRS stability.

In natural SRS, the angular characteristics (acute angle or obtuse angle) are usually regular. The rocks in sedimentary strata had fewer corners and their shape was spheroid; however, rocks in colluvial soil layers had sharp edges and spindle type shape (Liu et al. 2018a,b; Gao et al. 2016). Liu's studies (2018a,b; Lu et al. 2018; Tao et al. 2018) proved that the edge characteristics of rocks played a significant role on the strength and failure modes of soil–rock mixtures. When studying the stability of SRS with numerical method, scholars seldom consider the rock angular characteristic, which will underestimate or overvalue the SRS stability. In addition, the influence of the long axis inclination angles of rocks on SRS stability should not be ignored either, because the long axis inclination angles of rocks in SRS were usually regular, such as Chengdu subway was near 32.72° (Gao et al. 2016) and that in Three Gorges reservoir was near 60° (Shi et al. 2013). Based on the triaxial and in-situ test, Xu et al. (Wang et al. 2018; Zhang et al. 2016a,b) concluded that long axis inclination angles of rocks seriously affected SRS stability and failure modes, which should not be ignored in SRS stability analysis. Based on above analysis, it can be observed that the angular characteristics and long axis inclination angles of rocks should be considered in SRS stability analysis, which had not been systematically studied.

Based on above analysis, this paper has proposed a stochastic analytical method for the SRS stability with additional load considering the rock content, shape and long axis inclination angle. First, the identification and generation algorithms of rock geometry were described in detail. Then, the optimized random generation algorithm of SRS was introduced which could consider the interlock effect of rocks and corresponding random analytical models compared to Liu's algorithm (Liu et al. 2018a,b). Combining above algorithm and the finite element method, the influences of rock contents and long axis inclination angles on the SRS stability with additional load were studied. Finally, the reliability of the obtained numerical results was verified with experimental test results. The findings of this work can provide a reference for the design and reinforcement of SRS.

Shape characteristics of rocks

Angular characteristics of rocks

Based on Xu's research (2016a,b; Zhang et al. 2016a,b), it was witnessed that, due to the effect of the original bedrock characteristics, formation modes, degrees of weathering and

Fig. 1 Rock photography

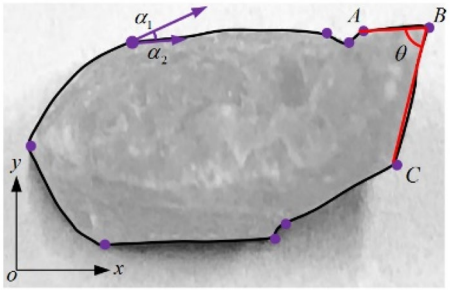

Fig. 2 Rock contour generated based on the color difference of rock and background

other factors, the rocks' angular characteristic was different, which played an important role on the SRS stability. In order to evaluate the sharpness of rock edges and corners, an identification algorithm was developed based on image recognition (Kamani and Ajalloeian 2020; Luo et al. 2019a,b). Figure 1 shows the photography of the sample rock used in this work and Fig. 2 shows its contour generated based on the color difference of rock and background (Liu et al. 2017). It should be observed that in photography process, two methods were employed to reduce the effect of rock shadows, including (1) the use of vertical irradiation of strong light source, which could make the color difference between the rocks, shadows and background panels more apparent; (2) the set of a smaller color recognition threshold, which can improve the recognition quality of rock contour. Then, a temporary axis system was created and rock contour was converted into point data. Tangent direction angle (α) of rock contour ($\vec{\alpha}_1$, $\vec{\alpha}_2$, $\vec{\alpha}_3$, …) was extracted in clockwise order and angle points were obtained according to threshold angle α_0. When α was larger than α_0, the point was recognized as rock angle point using Eq. (1).

$$\cos\alpha = \frac{\overrightarrow{\alpha_1}\cdot\overrightarrow{\alpha_1}}{\left|\overrightarrow{\alpha_1}\right|\left|\overrightarrow{\alpha_1}\right|} \tag{1}$$

After the recognition for rock points, rock angle points were labeled as A, B, C, D, etc. in clockwise order and

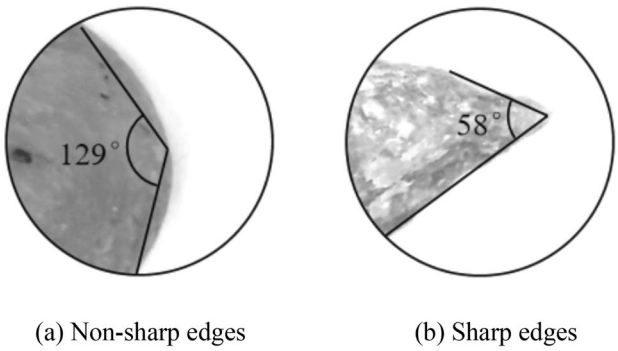

(a) Non-sharp edges (b) Sharp edges

Fig. 3 Typical rock angles

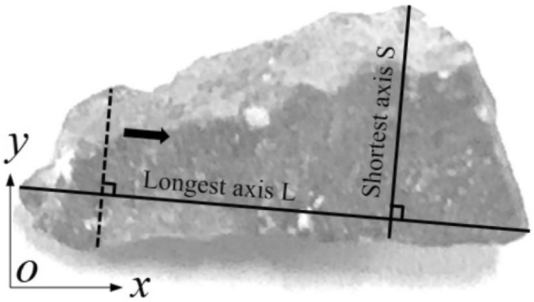

Fig. 4 Calculation model of ellipticity for rock

then the angle θ between adjacent edges was calculated using Eq. (2). The minimum value of θ was recognized as the characteristic angle of rock and two typical θ were shown in Fig. 3.

$$\cos\theta = \frac{\overrightarrow{BA}\cdot\overrightarrow{BC}}{\left|\overrightarrow{BA}\right|\left|\overrightarrow{BC}\right|} \tag{2}$$

Ellipticity characteristic of rocks

Pei et al. (2018) found that the geometric differences of rocks were mainly in their ellipticity (the ratio of short axis to long axis). The acquisition method of rock ellipticity in recognition algorithm is shown in Fig. 4.

As shown in Fig. 4, the longest L and shortest S axes of rock were found according to its angular point coordinates, and ellipticity k ($k = S/L$) was obtained based on these data. When the x axis of temporary coordinate system was parallel to that of global coordinate system, the angle m of the longest axis L with x axis was recognized as the angle of long axis of rock whose value was in the range of 0° to 180°.

The establishment of random SRS model

Based on Visual Basic for Applications (VBA) software, the generation of SRS contour was realized. The program was mainly divided into four parts, including input of original parameters, generation of rock polygon, intrusion detection of rocks and SRS generation.

Input of the initial parameters

The initial parameters of the input of the program mainly included six aspects, including slope boundary, gradation characteristics, ellipticity, long axis inclination, minimum internal angle and number of polygon sides. By setting different initial parameters, rocks with inconsistent rock geometry can be reflected in the calculation model as follows:

① Slope boundary: a closed polygonal contour was formed by coordinate points in Computer Aided Design (CAD) as a slope body.
② Gradation characteristics: rock content with a certain size range was input in which rock size was defined as mean value of the longest length L and the shortest length S for the rock.
③ Ellipticity: the value of ellipticity k was in range of 0 and 1.
④ Long axis inclination: long axis inclination angle of the rock was in range of 0° to 180° whose normal or average distribution could be selected.
⑤ Minimum internal angle θ: the value of this parameter was in the range of 20° to 90°.
⑥ Number of polygon sides B: which was above or equal to 3.

Generation of rock polygon

According to input rock characteristic parameter, a corresponding rock polygon was generated. Taking a 5-sided rock as example, as shown in Fig. 5, the following specific generation steps were taken:

① A random point P_1 (x_1, y_1) was generated within the boundaries of slope and a temporary coordinate system was established with P_1 as center;
② The angle θ_2 of the longest axis of rock was randomly generated within the set range and the longest length L was randomly generated according to input rock grading characteristics. Hence, long axis rock angular point coordinates P_2 and P_3 were obtained as follows:

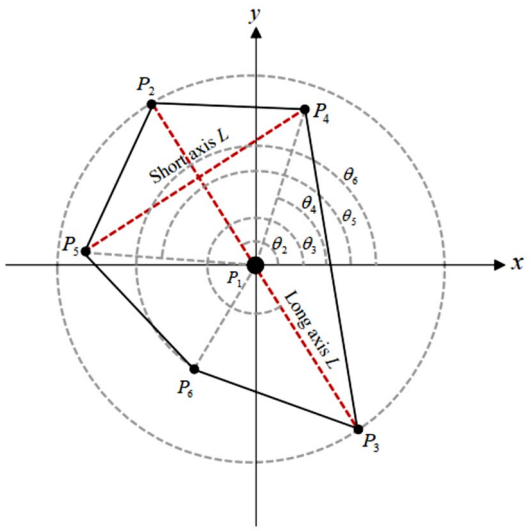

Fig. 5 The generation of a 5-side rock

$$P_2(x_1 + 0.5L\cos(\theta_2), y_1 + 0.5L\sin(\theta_2));$$

$$P_3 : (x_1 + 0.5L\cos(\theta_3), y_1 + 0.5L\sin(\theta_3)),$$

where $\theta_3 = \theta_2 + \pi$, $0 < \theta < \pi$;

③ Random angle θ_4 and length L_4 as well as point P_4 were obtained as follows:

$$(x_1 + 0.5L_4\cos(\theta_4), y_1 + 0.5L_4\sin(\theta_4)),$$

where $\theta_4 \neq \theta_2 \neq \theta_3$, $0 < \theta_4 < 2\pi$;

④ According to ellipticity k and known L, the length S of short axis was obtained. Considering that the longest axis L is vertical to the shortest axis S, the corresponding coordinates of angular point P_5 (L_5, θ_5) were calculated.
⑤ Random angle θ_6, length L_6 and point P_6 coordinates were obtained as follows:

$$(x_1 + 0.5L_6\cos(\theta_6), y_1 + 0.5L_6\sin(\theta_6)),$$

where $\theta_6 \neq \theta_2 \neq \theta_3 \neq \theta_4 \neq \theta_5$, $0 < \theta_6 < 2\pi$;

⑥ The inner angles of polygon were calculated according to the coordinates of each point; the minimum inner angle was found and it was compared with the design threshold. After meeting the requirements, the generation of a single rock was completed. Otherwise the following calculation procedure was repeated.

Checking for point intrusion

To avoid newly generated rock corners from being located inside the rock, area method was used to judge invasion

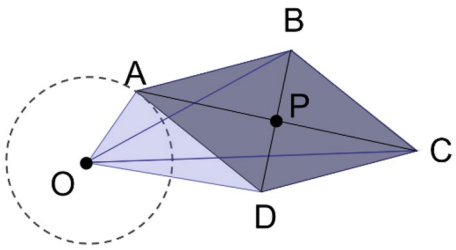

Fig. 6 Intrusion detection

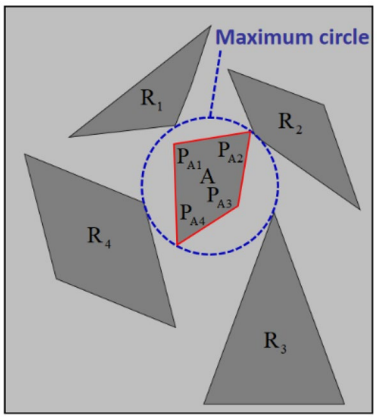

Fig. 7 The results of Liu's method (2018a,b)

characteristics between rocks, as shown in Fig. 6. The specific process of checking for point intrusion is as follows:

① A circle with a gradually increasing radius was generated with the newly generated point O as center.
② When the gradually expanding circle contacted the existing rocks, the contact point was defined as Point A, and the following rock points were labeled as B, C and D in clockwise order, as shown in Fig. 6.
③ According to the coordinates of each point, area of triangles OAB, OBC and OCD and finally that of S_{OABCD} were calculated.
④ Based on the center point P in long axis L, the area S_{ABCD} was obtained through the summation of triangles PAB, PBC, PCD and PDA.
⑤ Compare values of S_{OABCD} and S_{ABCD}; if equal, the point O is recognized as invading into the rock P.

Establishment of random SRS

For the generation of random rock contours, Liu et al. (2018a,b; Xu et al. 2016a,b) proposed a rock contour generation algorithm based on random circles. However, their algorithm ignored the "interlocking effect" between large

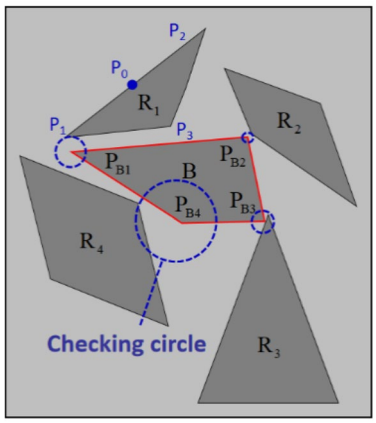

Fig. 8 The results of optimized algorithm

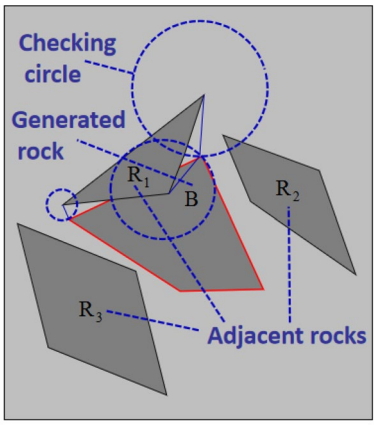

Fig. 9 Second intrusion judgment

rocks. In other words, the complementarity between rocks were not considered; the obtained results are shown in Fig. 7. Therefore, in this work an optimized rock contour generation algorithm was proposed considering interlocking effect between rocks by changing the order of rock invasion check procedures. The algorithm results and processes are shown in Figs. 8, 9 and 10.

As shown in Fig. 10, first some characteristic parameters of SRS were input and then, corresponding random points were generated according to input parameters. Intrusion judgment was made after each point was generated, as shown in Fig. 8. After all points were generated, they were connected to give a rock polygon. Then, the second intrusion judgment was conducted to ensure that the adjacent rocks (rocks R_1, R_2 and R_3) did not invade the generated rock (rock B), as shown in Fig. 9. Finally, ellipticity and minimum inner angle of rock polygon were

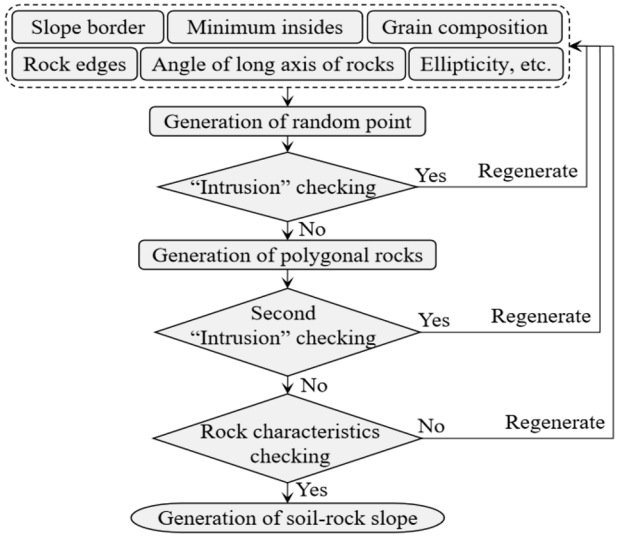

Fig. 10 The algorithm of SRS generation

checked. If the generated rock characteristic was satisfied, the establishment of SRS was finished. By the optimized rock contour generation algorithm, the SRS model which can consider interlock phenomenon was established.

Analytical models

The sizes of slope and rock

Characteristic sizes of slope

Based on a SRS in Three Gorges reservoir area (Fig. 11a), an analytical model of SRS with additional load was established, as shown in Fig. 11b. It should be observed that Fig. 11b is the calculation model simplified from Fig. 11a. The height of slope is 15 m, and the angle of slope is 45°.

For estimating the additional load on top of slope and avoiding partial failure at the top of slope, a loading board is set and the width is 5 m (which is a typical width).

Characteristic sizes of rocks

Napoli et al. (2018; Wang et al. 2017) found that 0.05 S_c (S_c is slope height) was a reasonable size threshold for soil and rock in the numerical analytical model, in which, the threshold definition of rock and soil was that a suitable size employed to distinguish rock and soil in terms of mechanical properties. Through numerical simulation, Liu et al. (2018a,b) found that 0.3 ~ 0.5 S_c was the threshold (S_c was the width of sliding surface at the top of slope in homogeneous soil). In order to fully consider the influence of rock distribution on the additional load of slope, combined with the calculation characteristic of MIDAS GTS/NX (finite element method) software, the size of the rock was defined as 2.5 m (0.5 S_c, which was the half width of loading plate).

Material properties

In FEM-based analytical models, the constitution of soil and rock is M-C constitution (Napoli et al. 2018), as shown in Table 1.

Table 1 The calculation parameters in model

Materials	Gravity (kN/m^3)	Elastic models (MPa)	Possion's ratio	Cohesion (kPa)	Friction angle (°)
Soil	19.0	105	0.35	14	22
Rock	26.4	2e4	0.2	1000	50

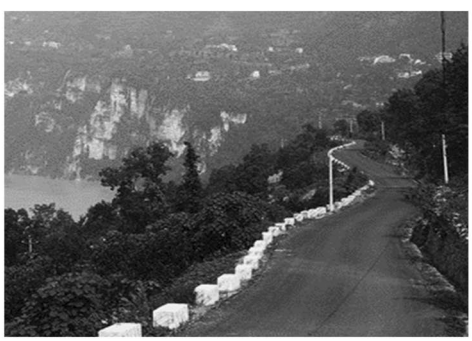

(a) SRS in Three Gorges reservoir area (copy from Internet)

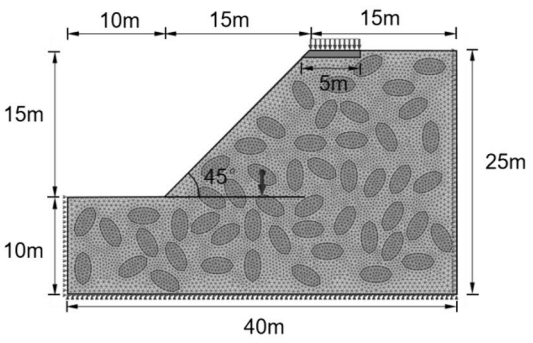

(b) Geometric model of SRS

Fig. 11 SRS model

Calculation of additional load in FEM

Li et al. (2016) studied the stability of SRS by FEM and limit analysis method. By comparing experimental failure mode and two software calculation results, FEM was found to be superior to limit analysis in the evaluation of the stability of SRS (Liu et al. 2018a,b). Therefore, FEM was used to study the stability of SRS in this article.

Strength reduction method is commonly used in slope stability analyses (Khorasani et al. 2019; Yang et al. 2019a,b). This method can obtain both specific safety factor and sliding zone of slopes. However, it cannot directly take into account the maximum additional loading of slopes. Therefore, using strength reduction method, ultimate slope load can be obtained by adjusting the load at the top of the slopes. When the safety factor of the slope is in the range of 0.99 ~ 1.01 (critical range of slope failure), the load is considered to be the additional load of slope.

Random models

Details about analyzing models with FEM

For computing the additional load of SRS accurately, the adaptive meshing method was adopted, where the meshes around rocks was smaller than the meshes of soil. Mesh size near and in the rocks is 30 times smaller than the rock perimeter for obtaining accurate simulation results, which threshold value can better reflect the influence of rocks with inconsistent geometry and interlock phenomenon on the slope in the simulation. As shown in Fig. 11, it was a meshing results of analyzing model with 40% rock content, in which 13,265 elements were divided. In terms of boundary conditions, the horizontal constraints were added at both sides of slope model, and the fixed constraints were added at the bottom of the slope model. For considering the difference of soil and rock in calculation, the properties of each material are assigned to corresponding elements. In addition, the gravity of each material (soil and rock) was added as the initial load before analyzing. It should be observed that, according to studies from Mohsen (2019) and Chen et al. (2019), the influence of the initial hydro-geological condition and permeability on SRS stability is also great, which will be systematically studied in the future research.

Random models considering different rock contents

Based on the statistics obtained by Shi et al. (2013; Zhang et al. 2018), the ellipticity (0.5) and shape characteristics (ellipse) of rocks in the landslide body of Three Gorges reservoir area and random rocks were set. 10, 20, 30, 40, 50 and 60% rock contents were evaluated by establishing 15 sets of stochastic models in which, the model for 60% rock content was hard to form by Liu's method (2018a,b) due to the interlock effect of rocks. Besides, the 15 sets of models are designed to fully consider the impact of rock distribution on SRS stability and obtain the statistical analysis results. The first group of analytical models is shown in Fig. 12 as representative. It should be pointed out that the rock distribution in numerical analysis is random.

Random models considering different long axis inclination angles for rocks

According to the statistical results of Gao et al. (2016; Shi et al. 2013), it could be concluded that the long axis inclination angles for rocks in one area were regular, which had a significant influence on the mechanical properties

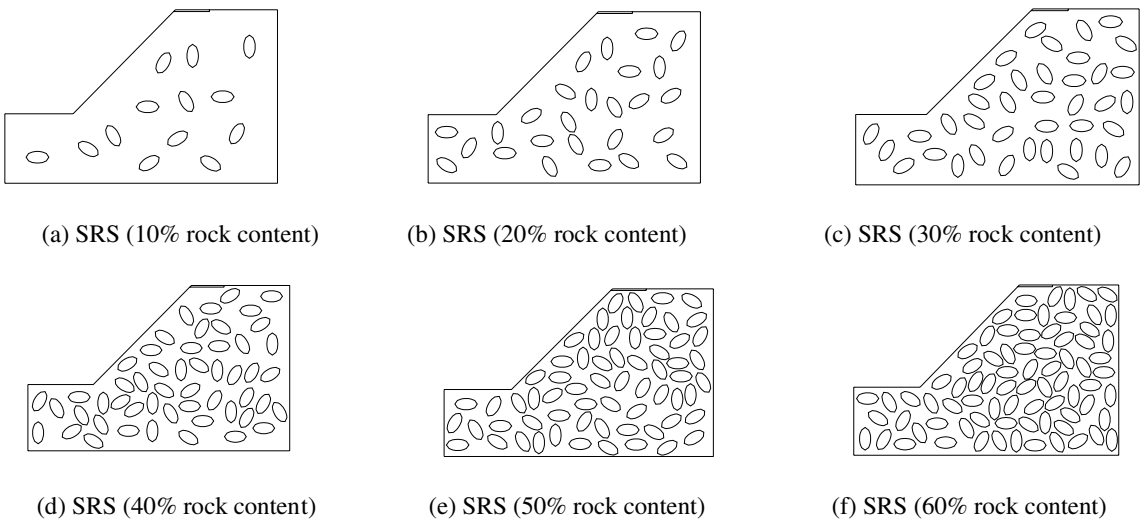

(a) SRS (10% rock content) (b) SRS (20% rock content) (c) SRS (30% rock content)

(d) SRS (40% rock content) (e) SRS (50% rock content) (f) SRS (60% rock content)

Fig. 12 SRS models taking into account different rock contents

of soil-rock mixtures (Gong and Jun 2017). However, less researches focused on the influence of long axis inclination angles for rocks on the slope stability. In this article, for studying the effects of long axis inclination angles for rocks to the additional load, the long axis inclination angles for rocks are set as same. Hence, 12 sets of random distribution models considering different long axis inclination angles for rocks were established at different rock contents (20, 40 and 60%), in which the long axis inclination of each model was adjusted by the rotation of the central axis of a single rock. Slope analysis models with 40% rock content and different long axis inclination angles (0°, 15°, 30°, 45°, 60°, 75°, 90°, 105°, 120°, 135°, 150° and 165°) are shown in Fig. 13.

Additional load analysis of SRS considering rock content

The additional load analytical results of SRSs considering different rock contents (0%~60%) are shown in Fig. 14.

Influence of rock distribution on plastic belt development

As shown in Fig. 14, according to the distribution of rocks, the plastic belt was not smooth and did not keep the arc shape any more. Combing with reference (Gong and Jun 2017; Liu et al. 2018a,b) and plastic belt in numerical analysis, four main influence modes of plastic belt development were proposed for the slope, as shown in Fig. 15, including detour, through, scatter and contain modes, and the corresponding affecting influence was detailed.

Detour mode: as shown in Fig. 15(a), (e), rocks were distributed on the path of the plastic belt of slope which could affect the length and developing directing of plastic pass. If rock distribution changed the development direction of the plastic belt of slope, the failure mode of slope was also changed, as shown in Fig. 14(c), which had a great impact on the additional load of slope. Plastic belt was developed along the edge of rock but did not change development direction. At this time, the presence of rock increased the length of the plastic belt and the additional load of slope, as shown in Fig. 14(b).

Through mode: as shown in Fig. 15(b), (f), some rocks were distributed on the development path of the plastic belt of slope and plastic belt developed through the rocks. When the slope was shear-deformed, the interlock effect of rocks was greatly increased the anti-sliding force and an additional load of slope.

Scatter mode: as shown in Fig. 15(c), (g), rocks were distributed on the development path of the plastic belt of slope and the single plastic belt entered the rock pile and developed into multiple plastic belts. The main plastic belt

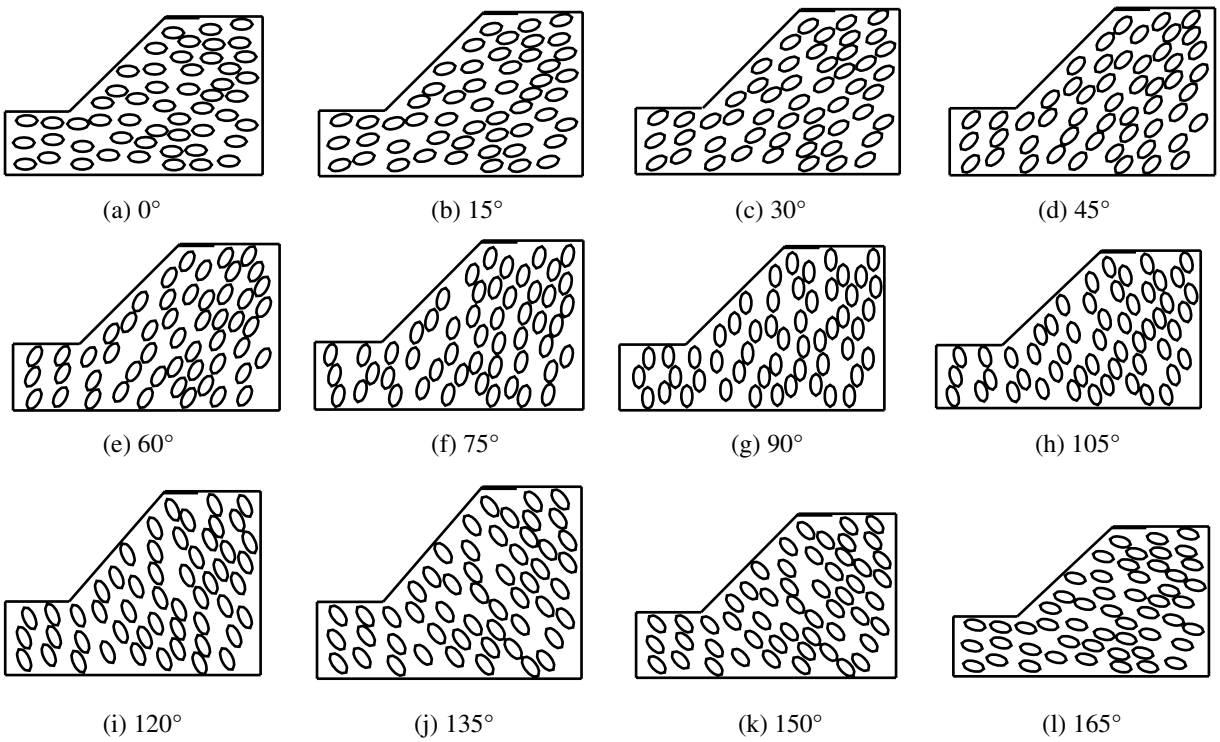

Fig. 13 Analytical models for different long axis inclination angles of rocks

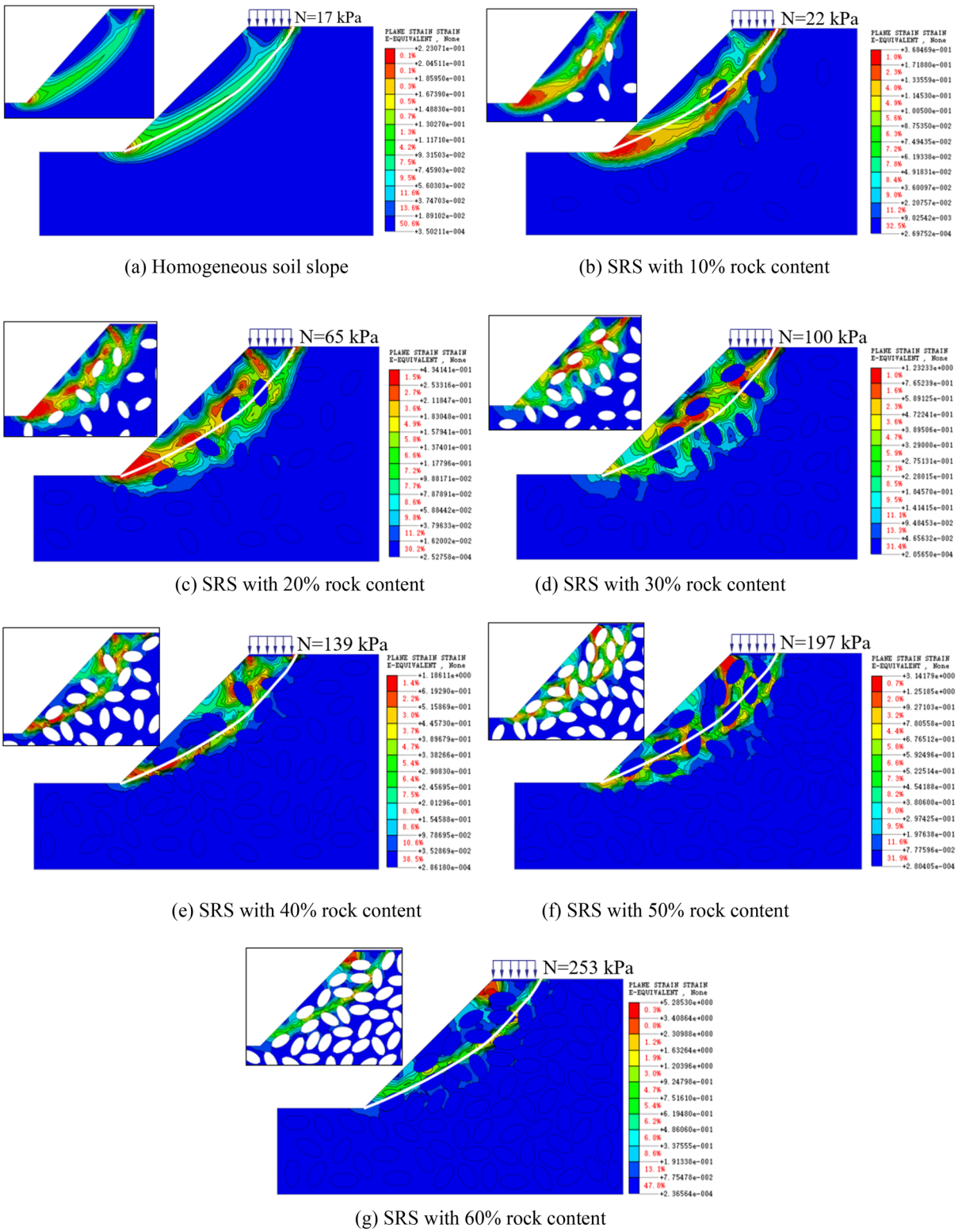

(a) Homogeneous soil slope

(b) SRS with 10% rock content

(c) SRS with 20% rock content

(d) SRS with 30% rock content

(e) SRS with 40% rock content

(f) SRS with 50% rock content

(g) SRS with 60% rock content

Fig. 14 The analytical results considering different rock contents

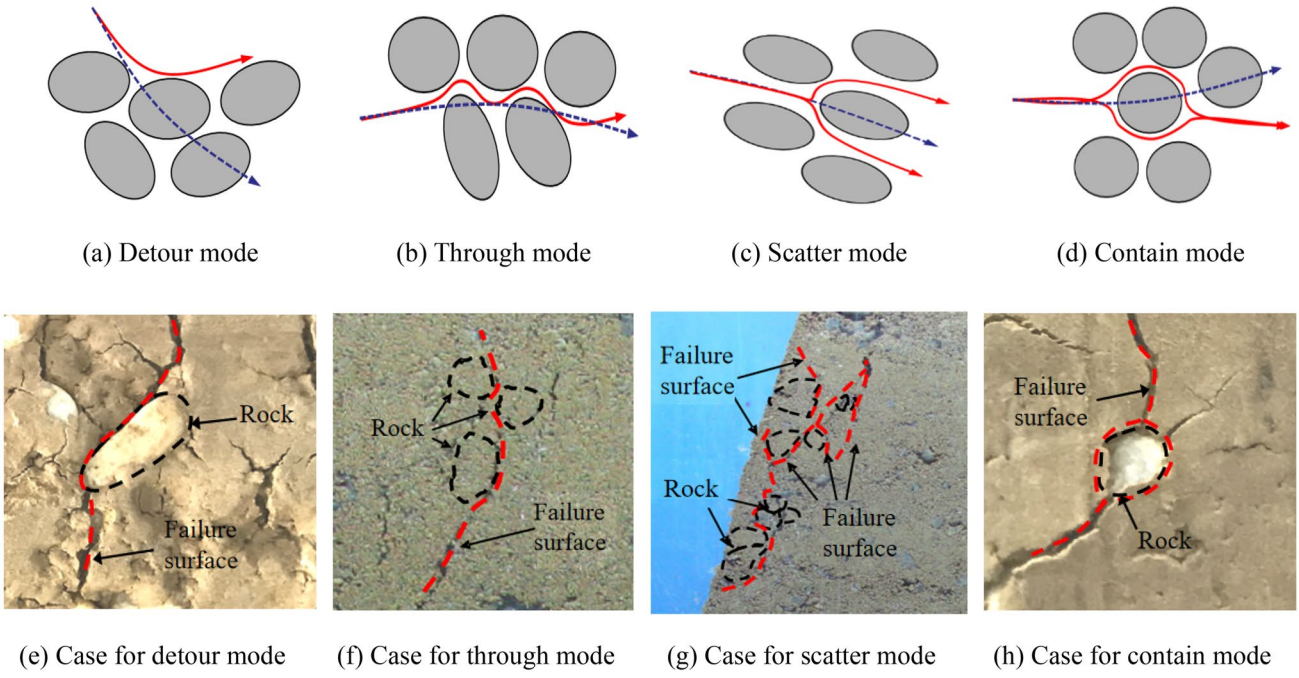

Fig. 15 4 typical types of plastic path (Gong and Jun 2017; Liu et al. 2018a,b)

developed into multiple sub-plastic belts and slope could not directly form a continuous main plastic belt, as shown in Fig. 14(h), increasing the additional loading of slope.

Contain mode: as shown in Fig. 15(d), (g), rocks were distributed on the development path of the plastic belt of slope which was developed along both sides of rocks. The distribution of rock made the plastic belt wider and longer which increased the additional load of slope to some extent.

SRS for different rock contents

As shown in Fig. 14, it could be found that, with the increase of rock content, the additional load of the slope was increased and the plastic development path of slope was affected more seriously by the rocks with the increase of rock content. As shown in Fig. 14(a), the top and foot of the slope formed main plastic bands which exhibited circular arc shape without any tortuosity.

In Fig. 14(b), 14 rocks appeared in the slope, and "detour mode" was the main influence mode. The path was offset to the inner side of slope and the length of plastic belt of slope was increased, which improved the anti-sliding force and increased additional load of the slope (5 kPa increase relative to homogeneous soil slope).

In Fig. 14(c), 27 rocks appeared in the slope and, due to the effect of rock distribution, plastic belt position of slope was changed. "Detour mode" was the main influence mode and, the plastic belt no longer along the inside of the top loading board to the foot of the slope, but from the both sides of the load board to the foot of the slope, which made the slope prone to produce shallow landslides on slope surface and showed "y" shape. The developing direction of plastic belt was changed and the additional load on slope top was increased to 65 kPa.

In Fig. 14(d), 40 rocks appeared in the slope and, due to rock distribution, plastic belt position of the slope was changed. "Detour and contain mode" were the main influence modes, and the plastic belt along the inside of the top load board to the middle of the slope, which easily led to partial landslides near slope top. The developing direction of plastic belt was changed and the plastic belt tended to be not smooth. Hence, the additional load of slope was increased to100 kPa.

In Fig. 14(e), 53 rocks appeared in the slope and, due to rock distributions, plastic belt at slope foot was developed along the gaps of rocks, in which, "Detour mode, scatter and contain mode" were the main influence modes. When deformation occurred, adjacent rocks produced high anti-sliding forces. Plastic belt development on slope top was complex that the developing direction of plastic belt was changed and the plastic belt tended to be not smooth. The additional load of slope was increased to 139 kPa.

In Fig. 14(f), 66 rocks appeared in the slope and rock distributions caused the plastic development path of slope to exhibit obvious "y" shape, in which, "detour, through, scatter and contain modes" all appeared. The plastic belt was developed along the edges of rocks, and the developing

direction of plastic belt was changed and the plastic belt tended to be not smooth. The additional load of slope was increased to 197 kPa.

In Fig. 14(g), 79 rocks appeared in the slope and the position of the main plastic belt of slope was changed, in which "detour and through modes" were the main influence modes. The plastic belt develops along the crevice between rocks and is tortuous. In addition, it could also be observed that the developing tendency of plastic belt is not along the rocks with less relative distance. Hence, it could be concluded that some rocks might be recognized as one big rock when distance between rocks was less in some special rock distribution conditions. The plastic belt tended to be not smooth and the developing direction of plastic belt was changed, which greatly increased the anti-sliding force of sliding body. Hence, the additional load of the slope was increased to 253 kPa.

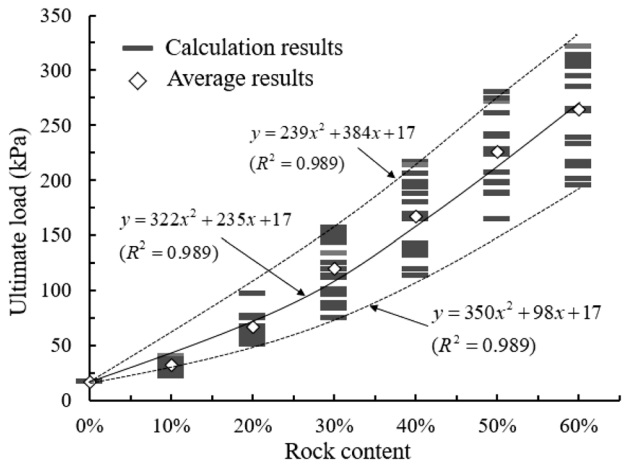

Fig. 16 The statistical results of additional load for SRS considering different rock contents (detailed in Table 3)

Statistical results of SRS considering different rock contents

As shown in Fig. 16 and Table 2, by analyzing the slope additional load in the 15-group analysis model, it was found that as rock content was increased, the additional load of slope was also increased. In addition, it can be observed that, due to the different random arrangement, the additional load of SRS is discrete, and the dispersion degree of additional load was increased with the increase of rock content. This tendency could be explained by the fact that, with the increase of rock content, the amount of rocks in the slope was increased, which (1) changed the length of plastic belt, (2) adjusted the smoothness of plastic belt, and (3) changed the developing direction of plastic belt. Hence, additional load was gradually increased (2019a,b).

For engineering reference, three fitting curves were obtained based on the average, minimum, and maximum values of additional load of slope at different rock contents and the correlation coefficients of all curves were larger than 0.980. In engineering, when estimating the additional load of SRS, it is advised to choose the three curves according to the importance factor of slope. The curve of maximum values is suitable for safety level three when the failure of slope only leads to economic losses. The curve of average values is suitable for safety level two when the failure of slope may lead to loss of life, personal injury and economic losses. The curve of minimum values is suitable for safety level one when the failure of slope can not only lead to loss of life, personal injury, economic losses but also cause serious secondary disasters.

Typical development modes of SRS plastic belt at 50% rock content

In terms of generality and complexity, 50% rock content is widely distributed in soil-rock slope. Besides, at this rock content, rock distribution has great influence on the slope stability and failure modes. Hence, in order to better support SRS engineering, four typical calculation models were selected which are shown in Fig. 17.

Table 2 The statistical results of additional load for SRS considering different rock contents

Rock content	0%	10%	20%	30%	40%	50%	60%	Describes
Mini-value (kPa)	17	22	51	75	113	164	195	The length of the plastic belt is shorter The plastic belt is relatively smooth The developing direction of plastic belt was changed
Maxi-value (kPa)	17	40	97	157	217	280	322	The length of the plastic belt is longer The plastic belt is not smooth The developing direction of plastic belt was changed
Difference between Mini-value and Maxi-value	0	18	46	82	104	116	127	The degree of dispersion was increased with the increase of rock content

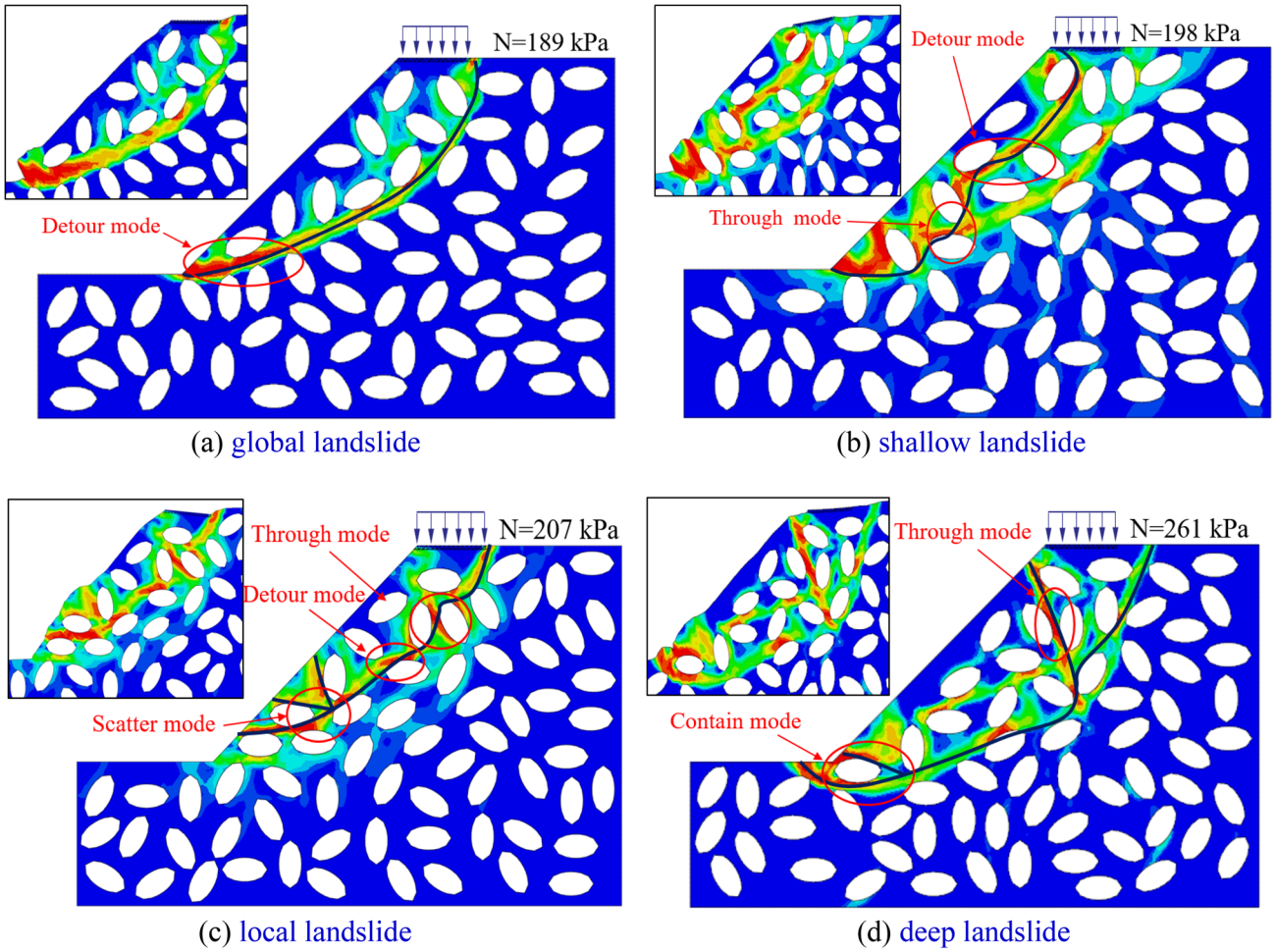

Fig. 17 Typical development modes of SRS plastic belt at 50% rock content

Figure 17 shows four typical development modes of SRS plastic belt at 50% rock content. It can be observed that due to the different rock distribution characteristic, the SRS shows different ultimate load and development modes of plastic belt. As shown in Fig. 17a, the ultimate load is 189 kPa, and the SRS tends to be global landslide. The plastic belt is developed from the foot of the slope to the inside of the loading plate, and the detour mode is the main development mode of plastic belt. In this landslide model, the sliding body tends to be complete because there is only one main plastic belt. As shown in Fig. 17b, the ultimate load is 198 kPa and the SRS tends to be shallow landslide. The plastic belt is developed from the foot of the slope to the outside of the loading plate. Detour mode and through mode are the main development modes of plastic belt. When this slope slides, the sliding body at the foot of the slope tends to be discrete due to the complex plastic belt at the foot of the slope. As shown in Fig. 17c, the ultimate load is 207 kPa and the SRS tends to be local landslide. The plastic belt is developed from the middle and lower part of the slope to inside of the loading plate. Detour mode, through mode and scatter modes are the main development modes of plastic belt. When this slope slides, the sliding body at the foot of the slope tends to disperse due to the development of plastic. As shown in Fig. 17d, the ultimate load is 261 kPa, and the SRS tends to be deep landslide. The plastic developed from the foot of the slope to both sides of the loading plate and showed a "y" shape. Through mode and contain modes are the main development modes of plastic belt. In this landslide model, due to the development of plastic belt, the sliding body are divided into two parts, and the sliding body near the foot of the slope tends to be dispersed. Based on above analysis and studies from Huang et al (2020), it can be concluded that the sliding body with scatter and contain modes and the sliding body with detour and through modes tend to be dispersed and complete, respectively.

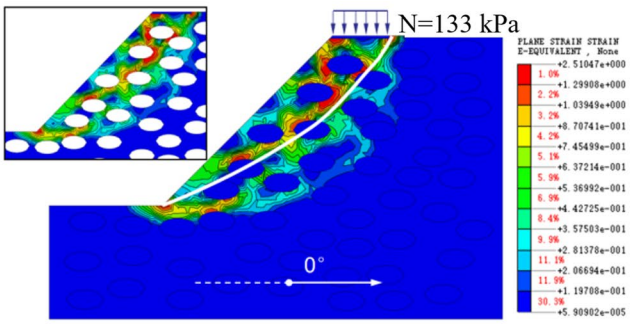

(a) 0° long axis inclination angles of rocks

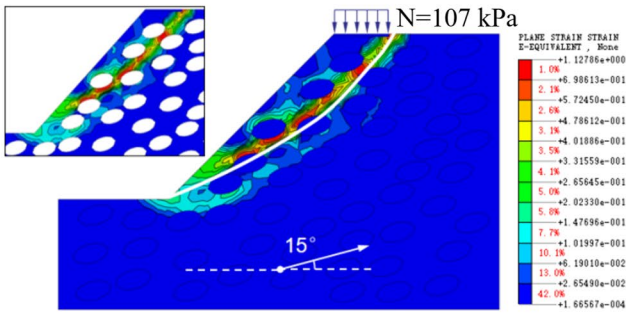

(b) 15° long axis inclination angles of rocks

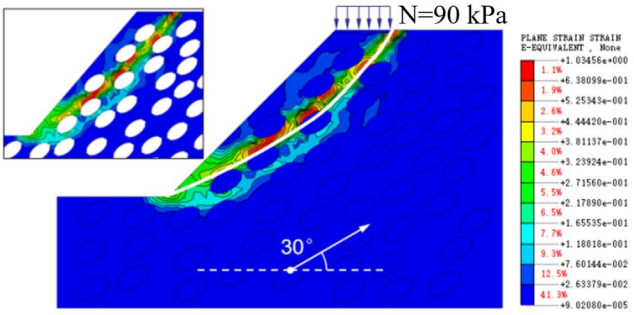

(c) 30° long axis inclination angles of rocks

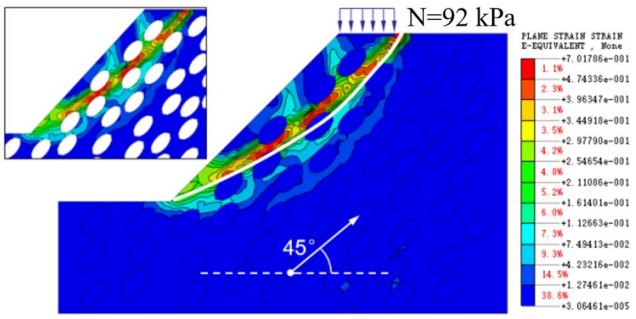

(d) 45° long axis inclination angles of rocks

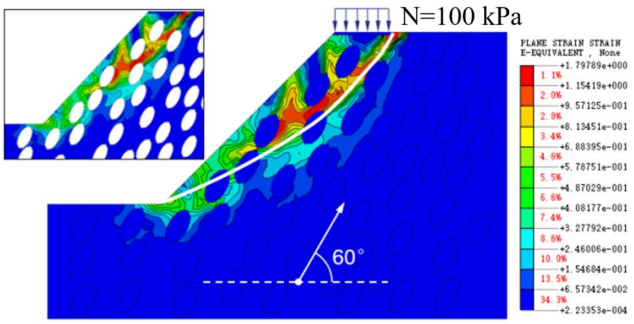

(e) 60° long axis inclination angles of rocks

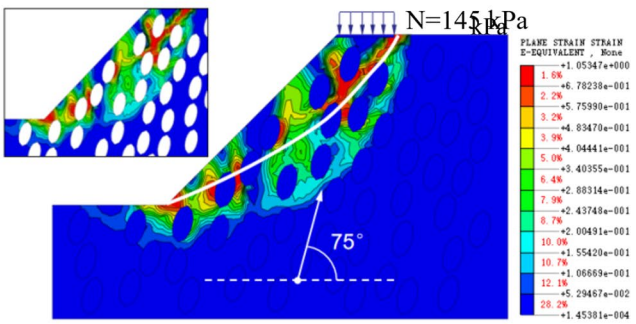

(f) 75° long axis inclination angles of rocks

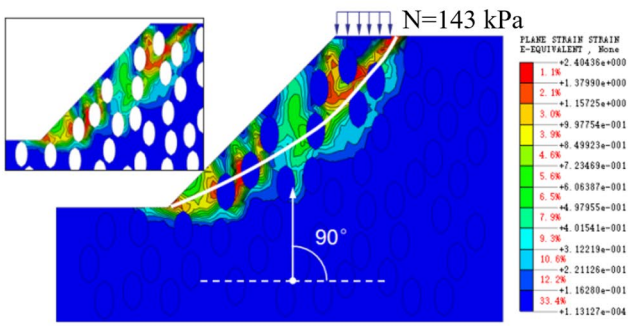

(g) 90°long axis inclination angles of rocks

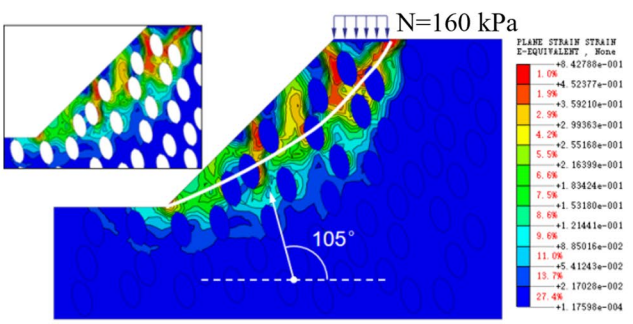

(h) 105° long axis inclination angles of rocks

Fig. 18 The analytical results of SRSs considering different rock long axis inclinations

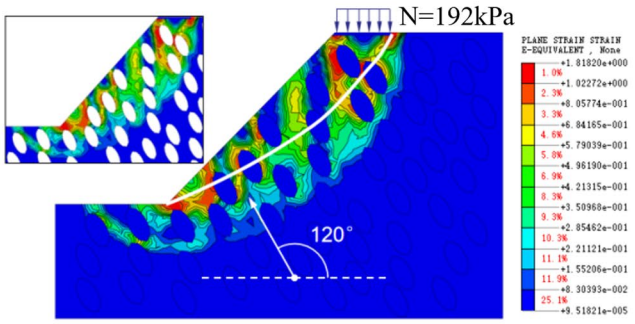

(i) 120° long axis inclination angles of rocks

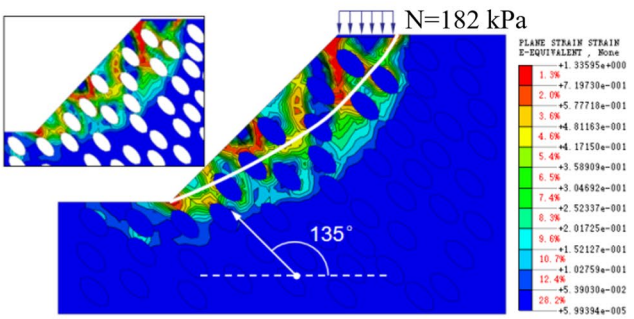

(j) 135° long axis inclination angles of rocks

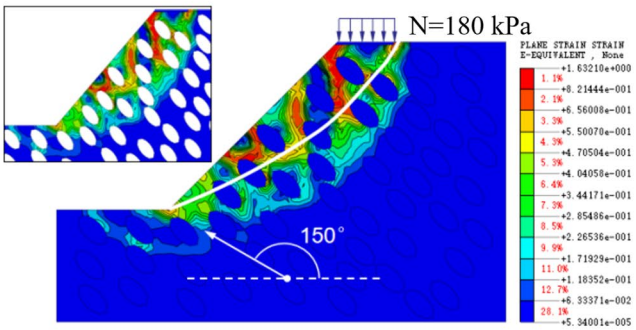

(k) 150° long axis inclination angles of rocks

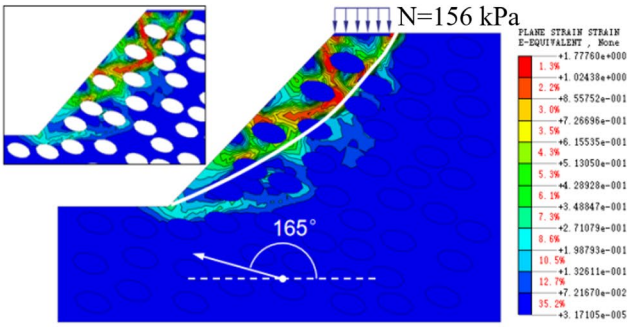

(l) 165° long axis inclination angles of rocks

Fig. 18 (continued)

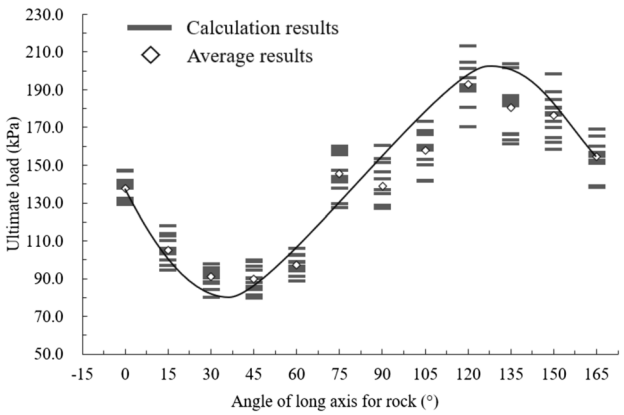

Fig. 19 The statistical analytical results of SRSs considering different rock long axis inclinations (40%, detailed in Table 4)

Additional load analysis of SRS considering long axis inclination angles of rocks

Slope stability analytical results of 40% rock content and different rock long axis inclination angles (0°, 15°, 30°, 45°, 60°, 75°, 90°, 105°, 120°, 135°, 150°, 165°) are shown in Figs. 18 and 19.

Results of SRSs with different long axis inclination angles of rocks

As shown in Fig. 19, with increase of long axis inclination angles of rocks in slopes the additional load of slope first decreased, then increased and finally decreased and exhibited "S" shape. The reason for this observation was related to the influence of the long axis of rocks on the plastic belt of slope.

As shown in Fig. 19, the additional load decreased with the increment of long axis inclination angles of rocks in range of 0° to 45°. It could be explained as shown in Figs. 18(a)–(d) that with the increase of long axis angels of rocks, plastic belts of slopes tended to be normalized which meant the slope easier formation of continuous main plastic belts in slopes, because the shear failure surface was tendency to develop along long axis of rocks. Therefore, additional load of slopes was reduced and minimum values were obtained between 30° and 45°.

It can also be found from Fig. 19 that additional load of slope increased with the increment of long axis inclination angles of rocks in the range of 45° to 135°. As shown in Fig. 18(e)–(j), with the increase of long axis inclination angles of rocks, the number of plastic belts was increased and plastic path tended to become complex and with more

plastic developing modes appearing, which prevented formation of a main plastic belt in slope. Therefore, additional load was increased and the maximum values were obtained between 120° and 135°.

As shown in Fig. 19, the additional load decreased with the increment of long axis inclination angles of rocks in the range of 135° to 180°. As shown in Fig. 18(k) to (i), with the increase of long axis inclination angles for rocks, the development direction of plastic belt was found to form local plastic belt in the top of slope. Hence, additional load was reduced in this angle range.

Statistical results of SRSs with different long axis inclination angles of rocks

As shown in Figs. 20 and 21, the changing tendency of additional load with long axis inclination angles at 20% and 60% rock contents was similar to that of 40% rock content, where

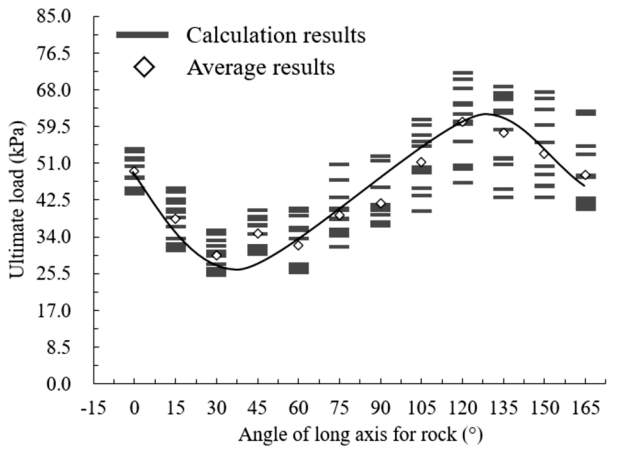

20% rock content (Detailed in Table A-3)

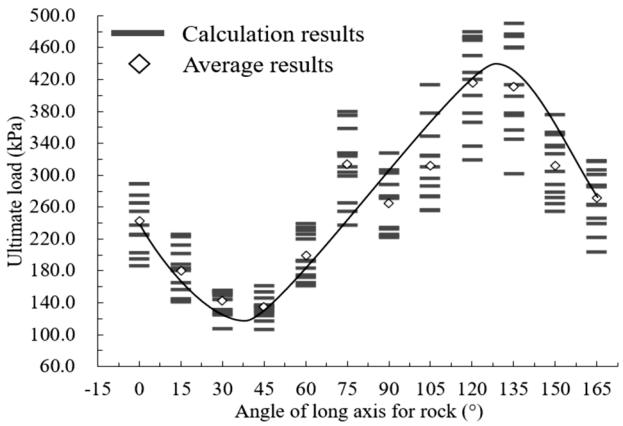

(b) 60% rock content (Detailed in Table A-4)

Fig. 20 The statistical analytical results of SRSs considering different rock long axis inclinations

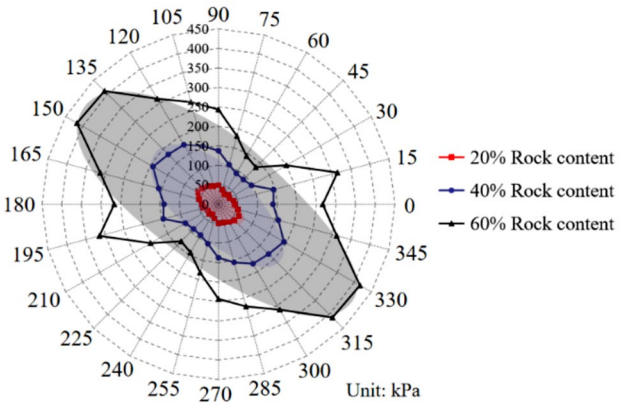

Fig. 21 The statistical analytical results of SRSs considering different rock long axis inclinations

the minimum value appeared in the range of 30° to 45° and the maximum value appeared in the range of 120° to 135°. Hence, combining the developing path of plastic belts, it was concluded that the minimum additional load appeared when long axis angel of rock was parallel to the direction of plastic belt developing, and maximum additional load value appeared when the angel was vertical to plastic belt development direction. This could be explained by the guiding effect of long axis of rocks on plastic belt development, which meant that plastic belt tended to develop along the long axes of rocks (Liu et al. 2018a, b).

The discrete ranges of additional load were from 26 to 73 kPa, 80 kPa to 204 kPa and 126 kPa to 459 kPa with discrete values of 47 kPa, 124 kPa and 333 kPa for 20%, 40% and 60% rock contents, respectively. Comparing discrete values with the predicted additional load 77, 162 and 274 kPa at 20%, 40% and 60% rock content, respectively, using equation $y = 322x^2 + 235x + 17$, the affecting rate of long axis inclination angles of rock to additional load can be obtained, which was 30.5%,38.3% and 60.8%. Hence, it can be concluded that long axis angle of rock should be considered in SRS and the affecting rate of long axis angle of rock increased with the increment of rock content.

Verification with physical models

By numerical method, it has been proved that the additional load of SRS and the discrete range increase with the increase of rock content and the minimum (or maximum) additional load appears when the long axis for rocks is parallel (or vertical) to the plastic belt. However, the obtained failure surface of SRS limited by the assumption of continuous element of FEM has some differences with the real, so the model tests were conducted, not only to verify the

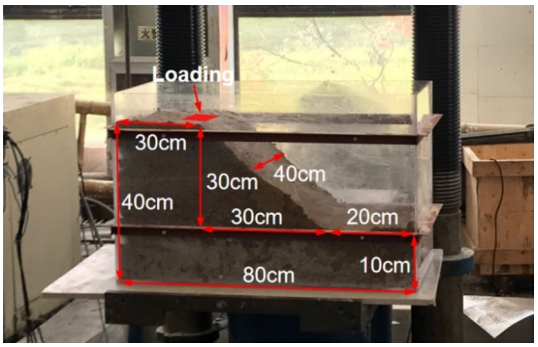

Fig. 22 Geometry of the model

(a) Slope before loading (b) Slope after loading

Fig. 23 Photographs of slope loading

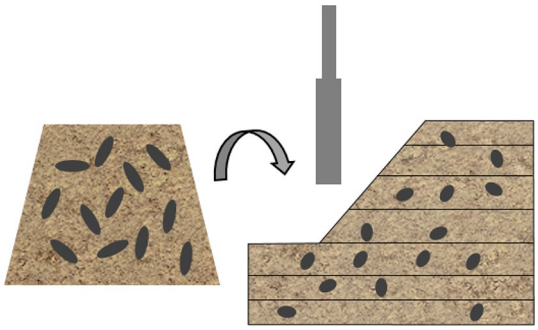

Fig. 24 Preparation of SRS considering different rock contents

Fig. 25 Part failure of SRS

conclusion in numerical analysis, but also to study the failure surface of SRS under additional load.

Details about model test

The model box was 80 cm long, 40 cm wide, and 50 cm high. The geometry of slope is shown in Fig. 22. The width of loading board on the top of slope was 10 cm and a large hydraulic machine was used for loading. Loading speed was set at 1 mm/min. Soil parameters were the same as those in numerical simulation shown in Table 1.

Slope structure before loading is shown in Fig. 23(a) and the results after loading are shown in Fig. 23(b). According to slope crack development degree during the loading process of homogeneous soil slope, 50 mm settlement or slide body formation was considered as the additional load of slope.

Model tests considering different rock contents

In the preparation of slope model, rock content was adjusted by controlling the mixed ratio of rock and soil. As shown in Fig. 24, it was important that the rocks were first mixed with soil and then the SRS was made, which was aimed to keep random characteristic for long axis inclination angles of rocks and rock distribution characteristic. When preparing slope model, the height of each layer should be controlled more than three times compared to the length of long axis of rocks, and the compacting power should be kept same. It should be observed that the use of same compacting equipment and the control of total compacting time (620 times) for each model were utilized to keep the compacting power.

The additional load of the obtained slopes at 0, 10, 20, 30, 40, 50 and 60% rock contents was 14.6, 15.2, 17.5, 18.9, 23.2, 31.2 and 36.4 kPa, respectively. It can be found that the

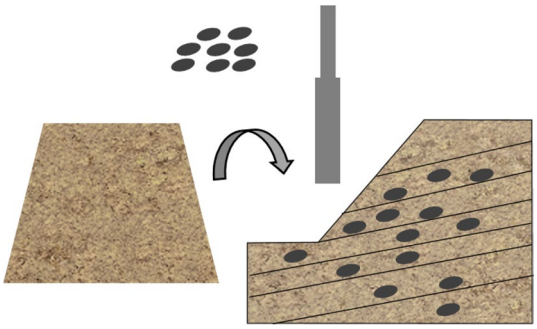

Fig. 26 Preparation of SRS considering different long axis inclination angles for rocks

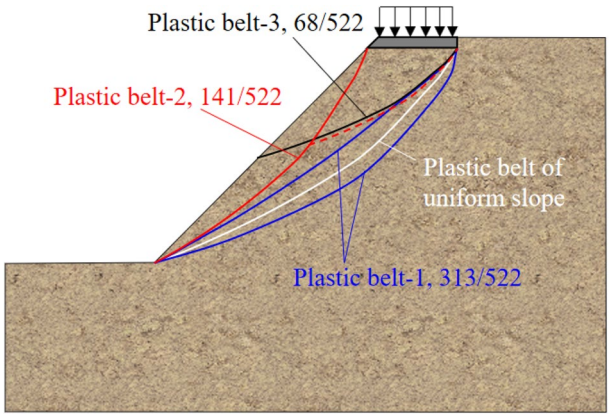

Fig. 27 3 typical plastic belt in SRS under top loading

additional load of slope increases with the increase of rock content, which is same to the tendency in numerical analysis. Therefore, it can be concluded that the additional load of SRS increases with the increase of rock content.

In addition, as shown in Fig. 25, a phenomenon could be observed that the failure surface path developed from the top of slope to the middle of slope when rock content is more than 40%, and the SRS showed part failure. Hence, it could be concluded that partial failure was more likely to happen than total failure in SRSs with high rock content (more than 40%).

Model tests considering different long axis inclination angles of rocks

For making the slope model considering long axis inclination angles for rocks, layered approaches and the preparing process for soil–rock mixtures were changed comparing to those that did not consider the long axis angle for rocks ("Model tests considering different rock contents"). When preparing as shown in Fig. 26, the angle of each layer is similar to the designed long axis inclination angles for rocks, and then rocks and soil are laid on the layer in turn, in which the height of each layer is smaller than 1.5 times height of the length of long axis for rocks. Under the characteristics of the oval shape of rocks and gravity, the long axis angle for rocks is similar to the angle of each layer.

At 40% rock content, the additional load increase values of slope at 0°, 38°, 90°, 128° and 165° long axis inclinations were 35.7, 17.6, 39.6, 47.7 and 34.2 kPa, respectively. The minimum and maximum additional load appeared at 38° and 128°, respectively, and this tendency was similar to the results in numerical analysis, which proved the importance to consider long axis inclination angles for rocks in SRS.

Typical failure surface of SRS under top loading

Based on the results of numerical analysis and physical tests, three typical potential plastic belts were put forward due to the rock distribution as shown in Fig. 27. According to the results of 522 statistical numerical models with different rock contents and long axis inclination angles of rocks, plastic belt-1 is recognised as the most common and there are 313 slopes showed this failure model. In this condition, the rock distribution usually changed the width and tortuosity of plastic belt. This failure mode is common in low rock contents (less than 40%) and long axis inclination angles for rocks from 15° to 75°.

Plastic belt-2 is a shallow failure of SRS, and there are 141 slopes showing this failure model. In this model, there are two kinds of plastic belts, in which, one plastic belt is developing from the toe of slope to the outer of the load board, and the other develops from the toe of the slope to the both sides of the load plate. This plastic belt usually appeared when rock content is high (over than 40%) and long axis inclination angles for rocks from 100° to 165°.

Plastic belt-3 is a partial failure of SRS, and there are 68 slopes showing this failure model. In this model, the plastic belt develops from the waist of slope to the inner of load plate. It is common in higher rock contents (more than 40%) and long axis inclination angles for rocks from 0° to 15°, 75° to 100° and 165° to 180°.

In addition, combing the achievements of Wang and Zhang (2019), some conclusions about sliding body for SRS can be obtained that, in high gravel content, the sliding body shows collapse when long axis inclination angles for rocks is vertical to the plastic belt due to the rotation or movement of rocks in slope. When long axis inclination angles for rocks is parallel to the plastic belt, the sliding body usually is whole due to the induction effect of the long axis of rocks to the development of plastic belts. The influence of rotation and movement of key rocks on the SRS will be studied in detail in the future research by combining corresponding experimental phenomenon.

Conclusion

Based on the characteristic parameters of rocks in SRS such as ellipticity, long axis angle and rock content, an improved stochastic algorithm of SRS was developed which could consider interlock effect between rocks. Then, the stability and additional load of SRSs were studied considering different rock contents and long axis inclination angles of rocks using the proposed algorithm and the following conclusions were drawn:

(1) A rock feature recognition method was put forward and, comparing with Liu's method, an improved stochastic algorithm was developed for SRSs which was able to well consider the effects of rock ellipticity, long axis inclination angles of rocks, rock contents and interlock effect between rocks.
(2) Based on plastic belts in the numerical analyzing models and physical models, four typical influence modes of rocks to the development of plastic belt were concluded, including detour, through, scatter and contain modes.
(3) According to 15 groups numerical analyzing models and physical models considering different rock contents, it was found that with the increase of rock content, the additional load of slope was also increased and larger discrete value appeared. Based on the statistical results of the additional load for SRS with 45°, the prediction equation was put forward for supporting engineering.
(4) According to 12 groups numerical analyzing models and physical models considering different long axis inclination angles for rocks, it was concluded that minimum or maximum additional load were, respectively obtained when long axis inclination angles of rocks were parallel with or vertical to plastic belt. The influence of long axis angle of rock in SRS should not be ignored due to the high impact effect to additional load (30.5%, 38.3% and 60.8% for 20% 40% and 60% rock content).
(5) Based on 522 numerical analyzing models and physical models, 3 typical development modes of plastic belt were concluded, which is corresponding to deep, shallow and part failure of SRS; furthermore, it is observed that the sliding body shows collapse (whole) modes when long axis inclination angles for rocks is vertical (parallel) to the plastic belt.

Finally, it should be pointed out that the influence of initial hydro-geological condition and permeability of the slope were not considered in this paper, which all had a significant influence on the SRS stability and failure modes. Besides, the influence of slope angle, the rotation of key rocks and the main influence modes of plastic belt development on the soil–rock slope has not been studied. Hence, in the future research, the effect of initial hydro-geological condition, permeability, slope angles and the rotation of key rocks on the SRS stability will be systematically studied.

Appendix

See Tables 3, 4, 5, and 6.

Table 3 Calculation results at random distribution of rocks

Rock content	Ultimate load of soil rock slope (kPa)														
	No. 1	No. 2	No. 3	No. 4	No. 5	No. 6	No. 7	No. 8	No. 9	No. 10	No. 11	No. 12	No. 13	No. 14	No. 15
0	17	–	–	–	–	–	–	–	–	–	–	–	–	–	–
10%	22	25	37	31	39	40	37	23	33	31	36	25	28	37	31
20%	64	51	97	75	77	54	52	58	75	76	55	64	77	59	67
30%	101	157	88	111	153	134	75	143	149	125	96	146	84	113	119
40%	138	217	113	132	188	214	142	137	206	164	180	198	193	119	169
50%	198	207	164	223	188	271	280	197	242	228	189	261	274	240	228
60%	265	213	217	233	195	322	314	303	201	310	239	305	285	295	263

Table 4 Calculation results at 40% rock content

Angle of long axis for rock (°)	No. 1	No. 2	No. 3	No. 4	No. 5	No. 6	No. 7	No. 8	No. 9	No. 10	No. 11	No. 12
0	133	141	138	147	133	139	139	131	129	147	142	131
15	105	105	113	118	95	110	106	103	97	94	100	114
30	88	87	91	80	93	92	94	98	96	96	96	84
45	90	95	97	88	80	86	84	100	86	99	90	82
60	99	91	94	103	102	99	94	96	97	95	106	89
75	143	144	144	141	130	155	157	159	147	160	128	138
90	143	154	137	135	128	127	127	129	147	129	161	152
105	160	158	167	141	153	166	150	153	168	173	161	142
120	192	181	201	196	193	204	191	170	190	190	213	192
135	182	204	187	186	185	161	202	167	163	182	183	166
150	180	170	177	199	158	178	189	162	165	181	173	185
165	155	151	157	152	169	160	166	153	155	139	160	138

Table 5 Calculation results at 20% rock content

Angle of long axis for rock (°)	No. 1	No. 2	No. 3	No. 4	No. 5	No. 6	No. 7	No. 8	No. 9	No. 10	No. 11	No. 12
0	54	45	48	54	52	48	50	45	54	44	52	44
15	31	36	40	38	45	42	34	32	40	32	43	44
30	32	30	25	33	35	31	30	25	26	27	36	28
45	35	37	40	38	32	31	30	39	31	37	37	32
60	27	27	26	28	26	36	36	40	41	34	26	39
75	47	34	35	38	32	36	38	43	41	35	51	40
90	40	37	37	53	46	41	36	52	41	38	39	41
105	49	40	50	58	56	55	49	45	60	61	44	50
120	68	51	50	65	71	72	62	56	65	47	60	61
135	51	66	52	59	66	69	43	52	63	45	67	63
150	43	48	50	67	50	66	46	43	60	56	46	63
165	62	42	48	42	55	48	53	43	41	40	63	41

Table 6 Calculation results at 60% rock content

Angle of long axis for rock (°)	No. 1	No. 2	No. 3	No. 4	No. 5	No. 6	No. 7	No. 8	No. 9	No. 10	No. 11	No. 12
0	203	187	275	226	290	266	266	238	255	290	196	226
15	143	182	227	214	223	189	158	145	142	166	203	184
30	149	157	126	156	133	153	155	108	144	128	154	150
45	128	135	147	154	138	130	162	125	118	136	108	134
60	240	193	175	193	221	184	235	227	173	231	161	166
75	266	304	359	311	329	376	300	380	329	324	255	238
90	289	329	275	223	308	235	272	303	273	227	224	233
105	258	379	296	256	275	349	287	413	273	311	325	324
120	337	401	451	320	378	421	473	481	474	429	470	367
135	302	346	375	357	461	399	474	460	477	491	378	413
150	256	339	327	336	351	289	279	265	305	377	355	273
165	285	263	222	319	317	308	240	205	264	288	301	246

Acknowledgements Special thanks to the anonymous reviewers and the editor for their useful suggestions on the manuscript.

Funding This research was funded by the National Natural Science Foundation of China (NO. 51778004, NO.51309121 and NO.51678300), Anhui Province University disciplines (professional) top-notch talent-funded projects, Excellent Young Talents Fund Program of Higher Education Institutions of Anhui Province (CN) (gxbjZD09).

Declarations

Conflict of interest The authors declare no conflict of interest.

References

Bao Y, Gao P, He X (2015) The water-level fluctuation zone of Three Gorges reservoir—a unique geomorphological unit. Earth Sci Rev 150:14–24. https://doi.org/10.1016/j.earscirev.2015.07.005

Chen T, Yang Y, Zheng H, Wu Z (2019) Numerical determination of the effective permeability coefficient of soil–rock mixtures using the numerical manifold method. Int J Numer Anal Met 43:381–414. https://doi.org/10.1002/nag.2868

Coli N, Berry P, Boldini D (2011) In situ non-conventional shear tests for the mechanical characterisation of a bimrock. Int J Rock Mech Min 48:95–102. https://doi.org/10.1016/j.ijrmms.2010.09.012

Gao M, Zhao J, Li S, Qiu Z (2016) Theoretical model of the equivalent elastic modulus of a cobblestone–soil matrix for TBM tunneling. Tunn Undergr Sp Technol 54:117–122. https://doi.org/10.1016/j.tust.2016.02.001

Gao W, Gao W, Hu R, Xu P, Xia J (2018) Microtremor survey and stability analysis of a soil-rock mixture landslide: a case study in Baidian town, China. Landslides 15:1951–1961. https://doi.org/10.1007/s10346-018-1009-x

Gong J, Jun L (2017) Influences of rock proportion on failure process and failure mode of soil-rock-mixture slope with PIV analysis. Rock Soil Mech 38(3):696–701. https://doi.org/10.16285/j.rsm.2017.03.011

He S, Ouyang C, Luo Y (2012) Seismic stability analysis of soil nail reinforced slope using kinematic approach of limit analysis. Environ Earth Sci 66(1):319–326. https://doi.org/10.1007/s12665-011-1241-3

Huang D, Gu DM (2017) Influence of filling-drawdown cycles of the Three Gorges reservoir on deformation and failure behaviors of anaclinal rock slopes in the Wu Gorge. Geomorphology 295:489–506. https://doi.org/10.1016/j.geomorph.2017.07.028

Huang XW, Yao ZS, Wang BH, Zhou AZ, Jiang PM (2020) Soil-rock slope stability analysis under top loading considering the nonuniformity of rocks. Adv Civ Eng 9575307:1–15. https://doi.org/10.1155/2020/9575307

Jiang S, Papaioannou I, Straub D (2018) Bayesian updating of slope reliability in spatially variable soils with in-situ measurements. Eng Geol 239:310–320. https://doi.org/10.1016/j.enggeo.2018.03.021

Kalender A, Sonmez H, Medley E, Tunusluoglu C, Kasapoglu KE (2014) An approach to predicting the overall strengths of unwelded bimrocks and bimsoils. Eng Geol 183:65–79. https://doi.org/10.1016/j.enggeo.2014.10.007

Kamani M, Ajalloeian R (2020) The effect of rock crusher and rock type on the aggregate shape. Constr Build Mater 41:117016. https://doi.org/10.1016/j.conbuildmat.2019.117016

Khorasani E, Amini M, Hossaini MF, Medley E (2019) Statistical analysis of bimslope stability using physical and numerical models. Eng Geol 254:13–24. https://doi.org/10.1016/j.enggeo.2019.03.023

Li D-Q, Xiao T, Cao Z-J, Phoon K-K, Zhou C-B (2016) Efficient and consistent reliability analysis of soil slope stability using both limit equilibrium analysis and finite element analysis. Appl Math Model. https://doi.org/10.1016/j.apm.2015.11.044

Liu Y, Zhou X, You Z, Yao S, Wang H (2017) Discrete element modeling of realistic particle shapes in stone-based mixtures through MATLAB-based imaging process. Constr Build Mater. https://doi.org/10.1016/j.conbuildmat.2017.03.037

Liu S, Huang X, Zhou A, Hu J, Wang W (2018a) Soil-rock slope stability analysis by considering the nonuniformity of rocks. Math Probl Eng 2018:1–15. https://doi.org/10.1155/2018/3121604

Liu Y, Xiao H, Yao K, Hu J, Wei H (2018b) Rock-soil slope stability analysis by two-phase random media and finite elements. Geosci Front 9:1649–1655. https://doi.org/10.1016/j.gsf.2017.10.007

Lu Y, Tan Y, Li X (2018) Stability analyses on slopes of clay-rock mixtures using discrete element method. Eng Geol 244:116–124. https://doi.org/10.1016/j.enggeo.2018.07.021

Luo J, Xu Z, Ren Z, Wang K, Tia L (2019a) Rock avalanche-debris geometry and implications for rock-avalanche genesi. Geomorphology. https://doi.org/10.1016/j.geomorph.2019.02.029

Luo J, Xu Z, Ren Z, Wang K, Tian L (2019b) Rock avalanche-debris geometry and implications for rock-avalanche genesis. Geomorphology 334:60–75. https://doi.org/10.1016/j.geomorph.2019.02.029

Manouchehrian A, Gholamnejad J, Sharifzadeh M (2013) Development of a model for analysis of slope stability for circular mode failure using genetic algorithm. Environ Earth Sci. https://doi.org/10.1007/s12665-013-2576-8

Meng QX, Wang HL, Xu WY, Cai M (2018) A numerical homogenization study of the elastic property of a soil-rock mixture using random mesostructure generation. Comput Geotech 98:48–57. https://doi.org/10.1016/j.compgeo.2018.01.015

Meng QX, Wang HL, Xu WY, Cai M (2019) Multiscale strength reduction method for heterogeneous slope using hierarchical FEM/DEM modeling. Comput Geotech 115:103164. https://doi.org/10.1016/j.compgeo.2019.103164

Mohsen M (2019) A general framework for coupled hydro-mechanical modelling of rainfall-induced instability in unsaturated slopes with multivariate random fields. Comput Geotech. https://doi.org/10.1016/j.compgeo.2019.103162

Napoli ML, Barbero M, Ravera E, Scavia C (2018) A stochastic approach to slope stability analysis in bimrocks. Int J Rock Mech Min 101:41–49. https://doi.org/10.1016/j.ijrmms.2017.11.009

Pei Z, Xiuli Du, Liu J, Dechun L, Qiuming G (2018) Study on the orientation angle of rock long axis on the macromechanical properties of soil-rock-mixture. Eng Mech 35:64–72. https://doi.org/10.6052/j.issn.1000-4750.2017.05.0362

Shi C, Chen KH, Wang SN, Haili W (2013) Research on microstructure statistical model of soil-rock mixture. Appl Mech Mater 353–356:28

Tao W, Sihong L, Yan F (2018) Compaction characteristics and minimum void ratio prediction model for gap-graded soil-rock mixture. Appl Sci 8(12):2584. https://doi.org/10.3390/app8122584

Vessia G, Kozubal J, Puła W (2017) High dimensional model representation for reliability analyses of complex rock–soil slope stability. Arch Civ Mech Eng 17:954–963. https://doi.org/10.1016/j.acme.2017.04.005

Wang T, Zhang G (2019) Failure behavior of soil-rock mixture slopes based on centrifuge model test. J Mt Sci 16:1928–1942. https://doi.org/10.1007/s11629-019-5423-x

Wang Y, Li X, Zheng B (2017) Stress-strain behavior of soil-rock mixture at medium strain rates—response to seismic dynamic loading. Soil Dyn Earthq Eng 93:7–17. https://doi.org/10.1016/j.soildyn.2016.10.020

Wang Y, Li CH, Hu YZ (2018) Use of X-ray computed tomography to investigate the effect of rock blocks on meso-structural changes in soil-rock mixture under triaxial deformation. Constr Build Mater 164:386–399. https://doi.org/10.1016/j.conbuildmat.2017.12.173

Wu LZ, Huang RQ, Xu Q (2015) Analysis of physical testing of rainfall-induced soil slope failures. Environ Earth Sci 73:8519–8531. https://doi.org/10.1007/s12665-014-4009-8

Xu W, Wang S, Zhang H, Zhang Z (2016a) Discrete element modelling of a soil-rock mixture used in an embankment dam. Int J Rock Mech Min 86:141–156. https://doi.org/10.1016/j.ijrmms.2016.04.004

Xu WJ, Hu LM, Gao W (2016b) Random generation of the meso-structure of a soil-rock mixture and its application in the study of the mechanical behavior in a landslide dam. Int J Rock Mech Min 86:166–178. https://doi.org/10.1016/j.ijrmms.2016.04.007

Yang Y, Sun G, Zheng H, Qi Y (2019a) Investigation of the sequential excavation of a soil-rock-mixture slope using the numerical manifold method. Eng Geol 256:93–109. https://doi.org/10.1016/j.enggeo.2019.05.005

Yang Y, Sun Y, Sun G, Zheng H (2019b) Sequential excavation analysis of soil-rock-mixture slopes using an improved numerical manifold method with multiple layers of mathematical cover systems. Eng Geol 1:105279. https://doi.org/10.1016/j.enggeo.2019.105278

Zhang Y (2017) Study on the strength/deformation characteristics and the interaction of rock and soil mixture. Rev Fac Ing 32(16):230–236

Zhang H, Xu W, Yu Y (2016a) Triaxial tests of soil–rock mixtures with different rock block distributions. Soils Found 56:44–56. https://doi.org/10.1016/j.sandf.2016.01.004

Zhang Z, Xu W, Xia W, Zhang H (2016b) Large-scale in-situ test for mechanical characterization of soil–rock mixture used in an embankment dam. Int J Rock Mech Min 4:317–322. https://doi.org/10.1016/j.ijrmms.2015.04.001

Zhang P, Jin L, Du X, Lu D (2018) Computational homogenization for mechanical properties of sand cobble stratum based on fractal theory. Eng Geol 232:82–93. https://doi.org/10.1016/j.enggeo.2017.11.013

Zhou AZ, Huang XW, Li N, Jiang PM, Wang W (2020) A monte carlo approach to estimate the stability of soil–rock slopes considering the non-uniformity of materials. Symmetry 4:590. https://doi.org/10.3390/sym12040590